PERGAMON

International Journal of Solids and Structures 39 (2002) 5683–5697

INTERNATIONAL JOURNAL OF SOLIDS and STRUCTURES

www.elsevier.com/locate/ijsolstr

SH-wave diffraction by an interfacial flaw in monoclinic bimaterials

L.M. Brock *, M.T. Hanson

Department of Mechanical Engineering, University of Kentucky, Lexington, KY 40506, USA

Received 13 March 2002; received in revised form 1 July 2002

Abstract

A system of incident, reflected and transmitted plane SH-waves is diffracted by an interface flaw in two dissimilar linearly elastic anisotropic half-spaces. The half-space solids have single planes of material symmetry. These coincide, but the two sets of principal material axes in the common plane have arbitrary orientations with respect to each other and to the interface.

Exact transient solutions show the effects of material properties and orientation. Increasing the degree of non-orthotropy causes the maximum and minimum shear wave speeds in each solid to deviate more from the isotropic limit. For a non-orthotropic/isotropic bimaterial, this also causes the dynamic stress intensity factor to decrease, and the factor always falls below the factor value arising for a homogeneous solid with properties identical to those of the isotropic constituent.

Keywords: Wave propagation; Non-orthotropy; Interface flaw; Diffraction; Stress intensity factor; Transient analysis

1. Introduction

Analyzing dynamic response to elastic waves is an accepted procedure for the characterization of laminates (Liu et al., 2001), and dynamic loading of laminates is an important design consideration (Ma et al., 2001). The presence of gaps, or flaws, in the interfaces between layers causes wave diffraction that can influence the results of such studies. Wave diffraction by interface flaws is also a stress-raising mechanism (Achenbach, 1973; Miklowitz, 1978) that can trigger delamination (Brock and Achenbach, 1973).

As the latter-most work attests to, studies of wave diffraction by interface flaws have often involved perfectly bonded (rigidly welded) isotropic bimaterials. In this article, therefore, diffraction of plane horizontally polarized shear (SH) waves by an interface flaw between two dissimilar linearly elastic anisotropic half-spaces with only single planes of material symmetry (Eshelby et al., 1953) is considered. The flaw is semi-infinite, and the single material symmetry planes of the half-space solids coincide. However, their

* Corresponding author. Tel.: +1-859-257-2839; fax: +1-859-257-8057.
E-mail address: brock@engr.uky.edu (L.M. Brock).

0020-7683/02/$ - see front matter
PII: S0020-7683(02)00423-7

principal material axes in the common plane have arbitrary orientations with respect to each other, the interface, and the travel direction of the incident wave.

Exact transient solutions for largely arbitrary incident plane SH-waves are obtained, and typical full-field expression for the anti-plane displacements in each solid presented. The dynamic stress intensity factor is also found. Both quantities are sensitive to both material properties and to principal material axis orientation. The degree to which the solids are non-orthotropic is especially important. The effect of properties and orientations is often most apparent in the interface shear wave speeds for each solid.

The study begins with the basic equations for the class of non-orthotropic solids with single planes of material symmetry. The diffraction problem is formulated, and exact solutions for both the plane wave assembly associated with the incident SH-wave and the scattered fields are presented. The insights gained on the effects of non-orthotropy are based both on the solution expressions and numerical calculations.

2. Basic equations

Consider a homogeneous linearly elastic solid characterized by the generalized Hooke's law (Sokolnikoff, 1956)

$$\begin{bmatrix} \sigma_{11} \\ \sigma_{22} \\ \sigma_{33} \\ \sigma_{32} \\ \sigma_{13} \\ \sigma_{21} \end{bmatrix} = \begin{bmatrix} c_{11} & c_{12} & c_{13} & 0 & 0 & c_{16} \\ c_{21} & c_{22} & c_{23} & 0 & 0 & c_{26} \\ c_{31} & c_{32} & c_{33} & 0 & 0 & c_{36} \\ 0 & 0 & 0 & c_{44} & c_{45} & 0 \\ 0 & 0 & 0 & c_{54} & c_{55} & 0 \\ c_{61} & c_{62} & c_{63} & 0 & 0 & c_{66} \end{bmatrix} \begin{bmatrix} \varepsilon_{11} \\ \varepsilon_{22} \\ \varepsilon_{33} \\ 2\varepsilon_{32} \\ 2\varepsilon_{13} \\ 2\varepsilon_{21} \end{bmatrix} \tag{1}$$

in terms of the Cartesian coordinates x_k $(k = 1, 2, 3)$, where $c_{ik} = c_{ki}$ are the elastic constants. Discussion of their relation to crystallographic properties is found in Nye (1957) and Theocaris and Sokolis (2000). The form of (1) shows that the Cartesian system defines the principal material coordinates, and that the x_1x_2-plane is a plane of material symmetry. The strains ε_{ij} and stresses σ_{ij} satisfy, in the absence of body forces,

$$2\varepsilon_{ij} = 2\varepsilon_{ji} = u_{i,j} + u_{j,i}, \quad \sigma_{ij,j} = \rho\ddot{u}_i, \quad \sigma_{ij} = \sigma_{ji} \tag{2}$$

Here ρ is the mass density, u_i is the displacement in the x_i-direction, $(\,)_{,j} \equiv \partial(\,)/\partial x_j$, and $(\dot{\cdot})$ signifies time differentiation. Eqs. (1) and (2) support the anti-plane state

$$u_1 = u_2 = u_{3,3} = 0, \quad \sigma_{11} = \sigma_{22} = \sigma_{33} = \sigma_{21} = 0 \tag{3}$$

and reduce to the system

$$\sigma_{32} = c_{44}u_{3,2} + c_{45}u_{3,1}, \quad \sigma_{13} = c_{55}u_{3,1} + c_{45}u_{3,2} \tag{4a}$$

$$\sigma_{13,1} + \sigma_{32,2} = \rho\ddot{u}_3 \tag{4b}$$

subject to the positive definiteness requirements (cf. Kraut, 1963; Payton, 1983)

$$(c_{44}, c_{55}) > 0, \quad c_{44}c_{55} - c_{45}^2 > 0 \tag{5}$$

No preference is given to either c_{44} or c_{55}, and $c_{45} = 0$ in the orthotropic limit (Sokolnikoff, 1956). It is convenient, therefore, to introduce the parameters

$$\bar{\mu} = \frac{1}{2}(c_{44} + c_{55}), \quad \bar{v} = \sqrt{\frac{\bar{\mu}}{\rho}} \tag{6}$$

and dimensionless ratios

$$\alpha = \frac{c_{55}}{\vec{\mu}}, \quad \beta = \frac{c_{44}}{\vec{\mu}}, \quad \gamma = \frac{c_{45}}{\vec{\mu}} \tag{7}$$

It is noted that (5) does not restrict the sign of c_{45}, and that γ represents, in effect, the degree of non-orthotropy in anti-plane strain. Eq. (6) defines an average shear modulus $\vec{\mu}$ and shear wave speed $\vec{v}$ in the x_1x_2-plane of material symmetry. In the isotropic limit (6) gives the single classical modulus and wave speed (Achenbach, 1973). In light of (6),

$$\alpha + \beta = 2, \quad (\alpha - 1)^2 + \gamma^2 = (\beta - 1)^2 + \gamma^2 = 1 - \Gamma \tag{8}$$

where the dimensionless quadratic

$$\Gamma = \alpha\beta - \gamma^2 \quad (0 < \Gamma < 1) \tag{9}$$

is useful in characterizing material behavior. Its upper bound in (9) arises because (α, β, γ) are real. Indeed, $\Gamma = 1$ only when $\alpha = \beta = 1$, $\gamma = 0$, i.e. in the isotropic limit $c_{44} = c_{55}$, $c_{45} = 0$.

3. Problem formulation

Consider two half-spaces of such materials, designated as solid 1 and solid 2. They are perfectly bonded along a semi-infinite portion of their interface; a vanishingly thin flaw separates them over the remaining portion. The solids are dissimilar, but each of their x_3-principal material axes is parallel to the flaw edge, i.e. their x_1x_2-planes of material symmetry coincide. In this common plane, however, the interface makes an arbitrary angle ϕ_k ($|\phi_k| < 180°$) with the x_1-principal axis of a solid k, where $\phi_1 \neq \phi_2$.

For convenience the single Cartesian system (x, y, z) in Fig. 1 is employed: The z-axis defines the flaw edge and $(y = 0, x < 0)$ and $(y = 0, x > 0)$ define, respectively, the flaw and the perfectly bonded interface. No generality is lost by placing solid 1 in half-space $y > 0$, and solid 2 in half-space $y < 0$. The xy-plane coincides with the common plane of material symmetry, and the (x, y)-axes are simple rotations of the

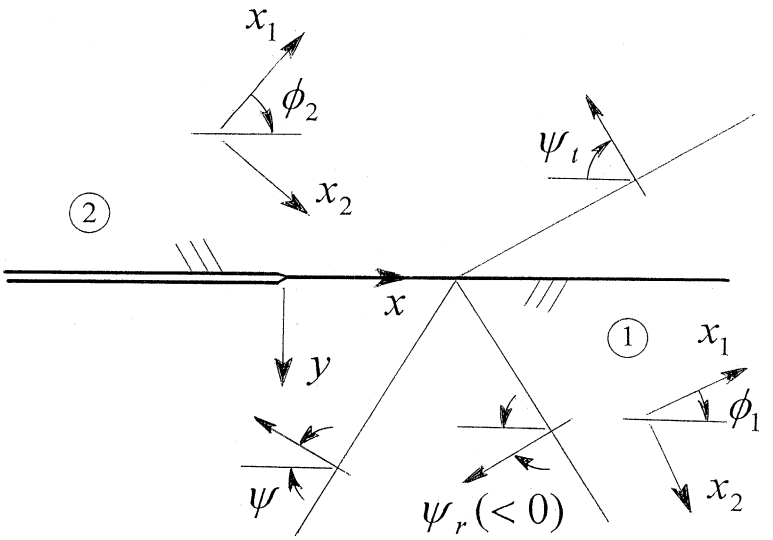

Fig. 1. Schematic of plane SH-wave system approaching flaw edge ($t < 0$).

principal material (x_1, x_2)-axes for a solid k through the angle ϕ_k. In view of (4a)–(9), with appropriate subscripts added, one can write the field equations

$$\frac{1}{\vec{\mu}_k}\sigma_{yzk} = C_k\frac{\partial w_k}{\partial x} + B_k\frac{\partial w_k}{\partial y}, \quad \frac{1}{\vec{\mu}_k}\ \sigma_{xzk} = A_k\frac{\partial w_k}{\partial x} + C_k\frac{\partial w_k}{\partial y} \tag{10a}$$

$$A_k\frac{\partial^2 w_k}{\partial x^2} + 2C_k\frac{\partial^2 w_k}{\partial x\,\partial y} + B_k\frac{\partial^2 w_k}{\partial y^2} = \frac{1}{\vec{v}_k^{\,2}}\ddot{w}_k \tag{10b}$$

for $y > 0$ $(k = 1)$ and $y < 0$ $(k = 2)$. Here $w_k(x, y, t)$ corresponds to u_3 in a solid k, t represents time, and formulas

$$A_k = 1 + \tfrac{1}{2}(\alpha_k - \beta_k)\cos 2\phi_k + \gamma_k \sin 2\phi_k \tag{11a}$$

$$B_k = 1 + \tfrac{1}{2}(\beta_k - \alpha_k)\cos 2\phi_k - \gamma_k \sin 2\phi_k \tag{11b}$$

$$C_k = \tfrac{1}{2}(\beta_k - \alpha_k)\sin 2\phi_k + \gamma_k \cos 2\phi_k \tag{11c}$$

define the tensor transformation (A_k, B_k, C_k) in a solid k of the array $(\alpha_k, \beta_k, \gamma_k)$ due to the rotation ϕ_k (cf. Eshelby et al., 1953). The formulas

$$\frac{\mathrm{d}A_k}{\mathrm{d}\phi_k} = -\frac{\mathrm{d}B_k}{\mathrm{d}\phi_k} = 2C_k, \quad \frac{\mathrm{d}C_k}{\mathrm{d}\phi_k} = B_k - 1 = 1 - A_k \tag{12a}$$

$$A_k + B_k = 2, \quad A_k B_k - C_k^2 = \Gamma_k \tag{12b}$$

are also useful, and it is noted that (12b) define invariants of the transformation.

Both solids are at rest when a horizontally polarized shear (SH) wave in solid 1 is for $t < 0$, as depicted in Fig. 1, incident upon the flaw at a travel angle of ψ with respect to the interface, where $0 < \psi < 90°$. This wave induces, in turn, reflected and transmitted plane SH-waves, with travel angle $(\psi_{\mathrm{r}}, \psi_{\mathrm{t}})$, respectively. The three-wave system reaches the flaw edge at $t = 0$ and is diffracted there. Linearity of (10a) and (10b) allows the superposition

$$w_1 = w_1^{\mathrm{s}} + w^{\mathrm{i}} + w^{\mathrm{r}} \quad (y > 0), \qquad w_2 = w_2^{\mathrm{s}} + w^{\mathrm{t}} \quad (y < 0) \tag{13a, b}$$

Here w_k^{s} is the scattered wave displacement field in a solid k, $(w^{\mathrm{i}}, w^{\mathrm{r}})$ is the incident and reflected wave field in solid 1, and w^{t} is the transmitted wave field in solid 2. All fields satisfy (10a) and (10b) and, in addition, the initial conditions

$$w_k^{\mathrm{s}} \equiv 0 \quad (t \leqslant 0) \tag{14}$$

hold, and continuity requires that

$$w^{\mathrm{i}} + w^{\mathrm{r}} = w^{\mathrm{t}} \tag{15a}$$

$$\sigma_{yz}^{\mathrm{i}} + \sigma_{yz}^{\mathrm{r}} = \sigma_{yz}^{\mathrm{t}} \quad (y = 0) \tag{15b}$$

Perfect bonding for $y = 0$, $x > 0$ and traction-free flaw surfaces for $y = 0$, $x < 0$ can then be imposed for $y = 0$, $t > 0$ as conditions

$$w_1^{\mathrm{s}} - w_2^{\mathrm{s}} = 0 \quad (x > 0) \tag{16a}$$

$$\sigma_{yz1}^{\mathrm{s}} = \sigma_{yz2}^{\mathrm{s}} = -\sigma_{yz}^{0} \quad (x < 0) \tag{16b}$$

Here σ^0_{yz} is given by either side of (15b). In addition, w^s_k should be finite for finite $t > 0$ and continuous in $y > 0$ $(k = 1)$ and $y < 0$ $(k = 2)$. Their gradients, however, may exhibit finite discontinuities at wavefronts, and integrable singularities at $(x, y) = 0$.

4. Plane wave system

The plane SH-wave system consists of the displacements

$$w^{\mathrm{i}} = \int_0^{\xi_{\mathrm{i}}} V(\xi)\,\mathrm{d}\xi, \qquad \xi_{\mathrm{i}} = t + \frac{x}{v}\cos\psi + \frac{y}{v}\sin\psi > 0 \quad (y > 0) \tag{17a}$$

$$w^{\mathrm{r}} = \int_0^{\xi_{\mathrm{r}}} V_{\mathrm{r}}(\xi)\,\mathrm{d}\xi, \qquad \xi_{\mathrm{r}} = t + \frac{x}{v_{\mathrm{r}}}\cos\psi_{\mathrm{r}} + \frac{y}{v_{\mathrm{r}}}\sin\psi_{\mathrm{r}} > 0 \quad (y > 0) \tag{17b}$$

$$w^{\mathrm{t}} = \int_0^{\xi_{\mathrm{t}}} V_{\mathrm{t}}(\xi)\,\mathrm{d}\xi, \qquad \xi_{\mathrm{t}} = t + \frac{x}{v_{\mathrm{t}}}\cos\psi_{\mathrm{t}} + \frac{y}{v_{\mathrm{t}}}\sin\psi_{\mathrm{t}} > 0 \quad (y < 0) \tag{17c}$$

where $(v, v_{\mathrm{r}}, v_{\mathrm{t}})$ are the travel velocities, and $(V, V_{\mathrm{r}}, V_{\mathrm{t}})$ are bounded and at least piecewise continuous. In light of (6), (10b) and (11a)–(11c)

$$v = \sqrt{A_{\mathrm{i}}}\,\vec{v}_1, \quad v_{\mathrm{r}} = \sqrt{A_{\mathrm{r}}}\,\vec{v}_1, \quad v_{\mathrm{t}} = \sqrt{A_{\mathrm{t}}}\,\vec{v}_2 \tag{18}$$

where the positive dimensionless quantities

$$A_{\mathrm{i}} = 1 + \tfrac{1}{2}(\alpha_1 - \beta_1)\cos 2(\phi_1 + \psi) + \gamma_1 \sin 2(\phi_1 + \psi) \tag{19a}$$

$$A_{\mathrm{r}} = 1 + \tfrac{1}{2}(\alpha_1 - \beta_1)\cos 2(\phi_1 + \psi_{\mathrm{r}}) + \gamma_1 \sin 2(\phi_1 + \psi_{\mathrm{r}}) \tag{19b}$$

$$A_{\mathrm{t}} = 1 + \tfrac{1}{2}(\alpha_2 - \beta_2)\cos 2(\phi_2 + \psi_{\mathrm{t}}) + \gamma_2 \sin 2(\phi_2 + \psi_{\mathrm{t}}) \tag{19c}$$

arise. The continuity condition (15a) and (15b) requires that

$$\frac{\cos\psi}{v} = \frac{\cos\psi_{\mathrm{r}}}{v_{\mathrm{r}}} = \frac{\cos\psi_{\mathrm{t}}}{v_{\mathrm{t}}} \tag{20a}$$

$$\frac{V_{\mathrm{r}}}{V} = \frac{C_1 + B_1\tan\psi - l(C_2 + B_2\tan\psi_{\mathrm{t}})}{l(C_2 + B_2\tan\psi_{\mathrm{t}}) - C_1 - B_1\tan\psi_{\mathrm{r}}} \tag{20b}$$

$$\frac{V_{\mathrm{t}}}{V} = \frac{B_1(\tan\psi - \tan\psi_{\mathrm{r}})}{l(C_2 + B_2\tan\psi_{\mathrm{t}}) - C_1 - B_1\tan\psi_{\mathrm{r}}} \tag{20c}$$

where (11a)–(11c) holds and the dimensionless ratios (Brock and Achenbach, 1973)

$$l = \frac{\vec{\mu}_2}{\vec{\mu}_1}, \quad m = \frac{\rho_1}{\rho_2} \tag{21}$$

are introduced. In view of (19a)–(19c), (20a) can be solved for the reflected and transmitted travel angles

$$2\psi_{\mathrm{r}} = -\tan^{-1}\frac{2\cos\psi\sqrt{A_{\mathrm{i}}B_1 - \Gamma_1\cos^2\psi}}{2\cos^2\psi - A_{\mathrm{i}}} - \tan^{-1}\frac{2C_1\cos^2\psi}{B_1 + C_1\sin 2\psi} \tag{22a}$$

$$2\psi_t = \tan^{-1}\frac{2\sqrt{lm}\cos\psi\sqrt{A_iB_2 - lm\Gamma_2\cos^2\psi}}{2lm\cos^2\psi - A_i} - \tan^{-1}\frac{2lmC_2\cos^2\psi}{A_i + 2(1-A_2)lm\cos^2\psi} \tag{22b}$$

in terms of the incident wave angle ψ. The argument of the radical in (22a) is non-negative for all $0 < \psi < 90°$, but existence of real values for (22b) when

$$lm\Gamma_2B_1 > \Gamma_1B_2 \tag{23}$$

requires the restriction

$$2\psi > \tan^{-1}\frac{2\sqrt{B_2}\sqrt{lm\Gamma_2B_1 - \Gamma_1B_2}}{lm(2B_2 - \Gamma_2)} - \tan^{-1}\frac{2B_2C_1}{lm\Gamma_2 + 2(1-A_1)B_2} \tag{24}$$

In the isotropic limit ($\alpha_k = \beta_k = 1, \gamma_k = 0$) results (17a)–(22b) reduce to those given by Brock and Achenbach (1973). Eqs. (20b) and (20c) can than be satisfied when

$$V(\xi) = \frac{T(\xi)}{\sqrt{\vec{\mu}_1\rho_1A_i}} \tag{25a}$$

$$V_r(\xi) = \frac{T(\xi)}{\sqrt{\vec{\mu}_1\rho_1A_i}}\frac{1}{D}\left[\frac{1}{\sqrt{A_i}}(C_i + \sin\psi) - \sqrt{\frac{l}{m}}\frac{1}{\sqrt{A_t}}(C_t + \sin\psi_t)\right] \tag{25b}$$

$$V_t(\xi) = \frac{T(\xi)}{\sqrt{\vec{\mu}_1\rho_1A_i}}\frac{B_1}{D}\left(\frac{\sin\psi}{\sqrt{A_i}} - \frac{\sin\psi_r}{\sqrt{A_r}}\right) \tag{25c}$$

Here $T(\xi_i)$ is the traction induced by the incident wave in solid 1. The dimensionless parameters (D, C_i, C_r, C_t) are

$$D = \sqrt{\frac{l}{m}}\frac{1}{\sqrt{A_t}}(C_t + \sin\psi_t) - \frac{1}{\sqrt{A_r}}(C_r + \sin\psi_r) \tag{26}$$

and, cf. (11a)–(11c) and (19a)–(19c),

$$C_i = \tfrac{1}{2}(\beta_1 - \alpha_1)\sin(2\phi_1 + \psi) + \gamma_1\cos(2\phi_1 + \psi) \tag{27a}$$

$$C_r = \tfrac{1}{2}(\beta_1 - \alpha_1)\sin(2\phi_1 + \psi_r) + \gamma_1\cos(2\phi_1 + \psi_r) \tag{27b}$$

$$C_t = \tfrac{1}{2}(\beta_2 - \alpha_2)\sin(2\phi_2 + \psi_t) + \gamma_2\cos(2\phi_2 + \psi_t) \tag{27c}$$

In view of (17a)–(22b), the traction field removed from the flaw surface by (16b) is

$$\sigma^0_{yz} = A_0T\left(t + \frac{x}{v}\cos\psi\right)\left(y = 0, x < 0, t + \frac{x}{v}\cos\psi > 0\right) \tag{28a}$$

$$A_0 = \sqrt{\frac{l}{m}}\frac{B_1}{D\sqrt{A_iA_t}}(C_t + \sin\psi_t)\left(\frac{\sin\psi}{\sqrt{A_i}} - \frac{\sin\psi_r}{\sqrt{A_r}}\right) \tag{28b}$$

where A_0 is a dimensionless traction amplitude factor.

5. Scattered waves: solution procedure

Conditions (16a) and (16b) can in view of (28a) be put in Wiener–Hopf (Achenbach, 1973) form:

$$w_1^s - w_2^s = W(x,t) \tag{29a}$$

$$\sigma_{yz1}^s = \sigma_{yz2}^s = \Sigma(x,t) - A_0 T\left(t + \frac{x}{v}\cos\psi\right) H(-x) \tag{29b}$$

Here $H(\,)$ is the Heaviside function, and (W,Σ) are, respectively, the interface flaw surface slip (relative displacement) and traction ahead of the flaw edge. Thus,

$$\Sigma \equiv 0 \quad (x<0) \tag{30a}$$

$$W \equiv 0 \quad (x>0) \tag{30b}$$

$$W \to 0 \quad (x \to 0-) \tag{30c}$$

and W is continuous for all $x<0$ except perhaps when the argument of T vanishes, and Σ may be integrably singular when $x \to 0+$. Application of unilateral (Sneddon, 1972) and bilateral (van der Pol and Bremmer, 1950) Laplace transforms

$$\hat{f}(x) = \int_0^\infty f(x,t)\mathrm{e}^{-pt}\,\mathrm{d}t \tag{31a}$$

$$\tilde{f} = \int_{-\infty}^{\infty} \hat{f}(x)\mathrm{e}^{-pqx}\,\mathrm{d}x \tag{31b}$$

where (p,q) are, respectively, positive real and imaginary, to (10a), (10b), (14), (29a) and (29b) gives

$$\tilde{w}_1^s = \frac{\vec{\mu}_2 a_2 \widetilde{W}\mathrm{e}^{-p\Omega_1 y}}{\vec{\mu}_1 a_1 + \vec{\mu}_2 a_2} \quad (y>0), \qquad \tilde{w}_2^s = \frac{-\vec{\mu}_1 a_1 \widetilde{W}\mathrm{e}^{-p\Omega_2 y}}{\vec{\mu}_1 a_1 + \vec{\mu}_2 a_2} \quad (y<0) \tag{32a}$$

$$-\frac{\vec{\mu}_1 a_1 \vec{\mu}_2 a_2 \widetilde{W}}{\vec{\mu}_1 a_1 + \vec{\mu}_2 a_2} = \widetilde{\Sigma} - \frac{A_0 \widehat{T}}{p(s_\psi - q)} \quad (y=0) \tag{32b}$$

In these equations

$$s_\psi = \frac{1}{v_\psi} = \frac{\cos\psi}{v} \tag{33a}$$

$$B_1\Omega_1 = C_1 q + a_1, \quad B_2\Omega_2 = C_2 q - a_2 \tag{33b}$$

$$a_k = \sqrt{\Gamma_k}\sqrt{s_k^2 - q^2}, \quad s_k = \frac{1}{(c_\mathrm{r}\vec{v})_k}, \quad c_{\mathrm{r}k} = \sqrt{\frac{\Gamma_k}{B_k}} \qquad (k=1,2) \tag{33c}$$

where (11a)–(11c) holds. Here $(s_k, c_{\mathrm{r}k}\vec{v}_k)$ are, respectively, the shear wave slowness and speed in a solid k along the interface, and (s_ψ, v_ψ) are, respectively, the plane wave system slowness and speed along the interface. In view of (6), (21) and (33b) the relation (23) that triggers restriction (24) arises when the interface shear wave speed in solid 2 exceeds that in solid 1 (source of the incident wave). In light of (22a)–(24),

$$s_\psi > \max(s_1, s_2) \tag{34}$$

Requiring $\mathrm{Re}(a_k) \geqslant 0$ in the q-plane with branches $\mathrm{Im}(q) = 0, |\mathrm{Re}(q)| > s_k$ guarantees that (32a) is bounded above.

Because (Σ, W) arise from the scattered wave field, their transforms exist for, respectively, $\mathrm{Re}(q) > -\min(s_1, s_2)$ and $\mathrm{Re}(q) < s_\psi$. The $\widehat{T}$-term in (32b) exists for $\mathrm{Re}(q) < s_\psi$, its singularity is isolated, and the coefficient of $\widetilde{W}$ is analytic in the strip $|\mathrm{Re}(q)| < \min(s_1, s_2)$. Therefore, a standard (Noble, 1958; Achenbach, 1973) decomposition process can be used to re-write (32b) in a form that equates a term that is analytic for $\mathrm{Re}(q) > -\min(s_1, s_2)$ to one that is analytic for $\mathrm{Re}(q) < s_\psi$. Because there is a common strip of analyticity, both terms are, by Liouville's theorem, equal to the same bounded entire function of (p, q). However, (30c) requires in light of (31b) that $pq\widetilde{W}$ be bounded as $|q| \to \infty$, which implies that the entire function is in fact zero. Two equations result and, for the case $s_2 > s_1$, can be solved to give

$$\widetilde{\Sigma} = \frac{A_0 \widehat{T}}{p(s_\psi - q)} \left[1 - \frac{G_+(s_\psi) a_2^+(q)}{G_+(q) a_2^+(s_\psi)} \right] \tag{35a}$$

$$\widetilde{W} = \frac{A_0 \widehat{T}}{\vec{\mu}_2 p^2} \left(1 + l \sqrt{\frac{\Gamma_2}{\Gamma_1}} \right) \frac{G_+(s_\psi) G_-(q)}{a_2^+(s_\psi) a_2^-(q)} \frac{1}{s_\psi - q} \tag{35b}$$

In (35a) and (35b) the quantities

$$\ln G_\pm(q) = \frac{1}{\pi} \int_{s_1}^{s_2} \tan^{-1} \frac{l a_2(\tau)}{a_1'(\tau)} \frac{\mathrm{d}\tau}{\tau \pm q} \tag{36a}$$

$$a_k^\pm(q) = \Gamma_k^{1/4} \sqrt{s_k \pm q}, \quad a_k'(q) = \sqrt{\Gamma_k} \sqrt{q^2 - s_k^2} \qquad (k = 1, 2) \tag{36b}$$

In (36b) $a_k^\pm$ are analytic in the overlapping regions $\mathrm{Re}(q) > -s_k$, $\mathrm{Re}(q) < s_k$. In (36a) $G_\pm$ are analytic in the overlapping regions $\mathrm{Re}(q) > -s_1$, $\mathrm{Re}(q) < s_1$, and

$$G_+(q) G_-(q) = \frac{a_1 + l a_2}{a_1 \left(1 + l \sqrt{\frac{\Gamma_2}{\Gamma_1}} \right)} \tag{37}$$

Results for $s_1 > s_2$ follow by replacing l with $1/l$ in (35a)–(37), interchanging the subscripts (1,2), and recognizing that the restriction (24) can now arise.

6. Maximum and minimum interface shear wave speeds

The interface shear wave speed parameters c_{rk} play a key role in (32a)–(37). In light of (12a) and (12b) it can be shown that they achieve extremal values $c_k^\pm$ for the principal material axis orientations $(\phi_k^\pm, \phi_k^+ - 180°, \phi_k^- + 180°)$. For $\gamma_k \geqslant 0$,

$$\phi_k^\pm = \tan^{-1} \frac{1}{\gamma_k} \left[\frac{1}{2} (\beta_k - \alpha_k) \pm \sqrt{1 - \Gamma_k} \right] \tag{38a}$$

$$c_k^\pm = \sqrt{1 \pm \sqrt{1 - \Gamma_k}} \tag{38b}$$

In Table 1 (Panels A and B) values of (38a) are given for various (positive) values of γ_k for, respectively, the cases $(\alpha_k = \beta_k, \beta_k = 2\alpha_k)$. The corresponding maximums and minimums (38b) are also given. The entries show that increasing the degree of non-orthotropy γ_k increases the maximum interface shear wave speed (c_k^+) beyond the isotropic limit $(c_k^\pm = 1)$, but lowers the minimum (c_k^-) below the limit. In Table 1 (Panel A)

Table 1
Maximum (+) and minimum (−) shear wave speed parameters and orientations

γ_k	Γ_k	ϕ_k^+ (°)	c_k^+	ϕ_k^- (°)	c_k^-
Panel A: $\alpha_k = \beta_k$					
0.05	0.9975	45	1.0247	−45	0.9747
0.1	0.99	45	1.0488	−45	0.9478
0.25	0.9682	45	1.0854	−45	0.9065
0.5	0.866	45	1.1687	−45	0.7962
0.75	0.6614	45	1.2577	−45	0.6466
0.9	0.4359	45	1.3234	−45	0.4989
Panel B: $\beta_k = 2\alpha_k$					
0.05	0.8864	85.7	1.1563	−4.7	0.8142
0.1	0.8789	81.7	1.161	−8.3	0.8075
0.25	0.8264	71.6	1.1902	−18.4	0.7638
0.5	0.6389	61.9	1.2653	−28.1	0.6317
0.75	0.3264	57	1.3493	−33	0.4234
0.9	0.0789	55.2	1.3999	−34.8	0.2007

$\phi_k^{\pm} = \pm 45°$ always, but Table 1 (Panel B) shows that increasing γ_k causes a greater deviation between the principal material axes and the interface. The orientations $\phi_k^{\pm}$ differ by 90° in both tables.

7. Scattered wave full fields

Combining (35b) with (32a) gives the scattered wave displacement transforms. The inversion operation for (31b) is (van der Pol and Bremmer, 1950)

$$\hat{f}(x) = \frac{p}{2\pi \mathrm{i}} \int \tilde{f} \mathrm{e}^{pqx}\, \mathrm{d}q \tag{39}$$

where integration is along a Bromwich contour. A standard (de Hoop, 1960; Brock and Achenbach, 1973) technique changes this contour to one in the complex q-plane that gives an integrand that has the form of the unilateral transform operation (31a). The scattered field follows by inspection. For an incident step-stress pulse $T(\xi) = T_{\mathrm{i}} H(\xi)$, the result for $(y > 0, s_2 > s_1)$ is

$$\begin{aligned} w_1^{\mathrm{s}} = {} & \frac{A_0 T_{\mathrm{i}}}{\pi \vec{\mu}_1} \frac{G_+(s_\psi)}{a_2^+(s_\psi)} \int_{s_1 r_1}^{t} \mathrm{Re}\left[\frac{a_2^+(q_1)}{G_+(q_1)} \frac{1}{s_\psi - q_1}\right] \frac{(t-\tau)\,\mathrm{d}\tau}{\sqrt{\Gamma_1}\sqrt{\tau^2 - s_1^2 r_1^2}} \\ & + \frac{A_0 T_{\mathrm{i}}}{\sqrt{\vec{\mu}_1 \rho_1}} \sqrt{\frac{A_{\mathrm{i}}}{B_1}} \frac{(t-t_1)H(t-t_1)}{\sqrt{A_{\mathrm{i}} - c_{r1}^2 \cos^2\psi}} \quad \left(x - \frac{C_1}{B_1} y + \frac{c_{r1} r_1}{\sqrt{A_{\mathrm{i}}}} \cos\psi < 0\right) \end{aligned} \tag{40}$$

The result for $(y < 0, s_2 > s_1)$ is

$$\begin{aligned} w_2^{\mathrm{s}} = {} & -\frac{A_0 T_{\mathrm{i}}}{\pi \vec{\mu}_2} \frac{G_+(s_\psi)}{a_2^+(s_\psi)} \int_{s_2 r_2}^{t} \mathrm{Re}\left[\frac{a_2^+(q_2)}{G_+(q_2)} \frac{1}{s_\psi - q_2}\right] \frac{(t-\tau)\,\mathrm{d}\tau}{\sqrt{\Gamma_2}\sqrt{\tau^2 - s_2^2 r_2^2}} + \frac{A_0 T_{\mathrm{i}}}{\pi \vec{\mu}_1} \frac{G_+(s_\psi)}{a_2^+(s_\psi)} \\ & \times \int_{t_h}^{s_2 r_2} \frac{\Delta(q_h) G_+(q_h)}{s_\psi - q_h} \frac{(t-\tau)H(t-\tau)\,\mathrm{d}\tau}{\sqrt{\Gamma_2}\sqrt{s_2^2 r_2^2 - \tau^2}} \quad \left(x - \frac{C_2}{B_2} y > \frac{s_2}{s_1} r_2\right) \\ & - \frac{A_0 T_{\mathrm{i}}}{\sqrt{\vec{\mu}_2 \rho_2}} \sqrt{\frac{A_{\mathrm{i}}}{B_2}} \frac{(t-t_2)H(t-t_2)}{\sqrt{A_{\mathrm{i}} - c_{r2}^2 \cos^2\psi}} \quad \left(x - \frac{C_2}{B_2} y + \frac{c_{r2} r_2}{\sqrt{A_{\mathrm{i}}}} \cos\psi < 0\right) \end{aligned} \tag{41}$$

In (40) and (41) it is understood that integrals vanish when the lower limit exceeds the upper limit. The q_k $(k = 1, 2)$ is the complex Cagniard contour parameterization

$$r_k^2 q_k = -\left(x - \frac{C_k}{B_k} y\right)\tau + \mathrm{i}\frac{\sqrt{\Gamma_k}}{B_k}|y|\sqrt{\tau^2 - s_k^2 r_k^2}, \quad r_k = \sqrt{\left(x - \frac{C_k}{B_k} y\right)^2 + \frac{\Gamma_k}{B_k^2} y^2} \tag{42}$$

Result (41) also has a purely real Cagniard contour parameterization and integrand:

$$r_2^2 q_h = -\left(x - \frac{C_2}{B_2} y\right)\tau + \frac{\sqrt{\Gamma_2}}{B_2} y\sqrt{s_2^2 r_2^2 - \tau^2} \tag{43a}$$

$$\Delta(q) = \left(1 + l\sqrt{\frac{\Gamma_2}{\Gamma_1}}\right)\frac{a_2^+(q) a_2(q) a_1'(q)}{l^2\Gamma_2(s_2^2 - q^2) + \Gamma_1(q^2 - s_1^2)} \tag{43b}$$

The first terms in (40) and (41) represent scattered waves that radiate from the flaw edge in the expanding regions $(y > 0, t > s_1 r_1)$ and $(y < 0, t > s_2 r_2)$, respectively. The limits imposed on (x, y) identify the last terms in (40) and (41) as signals that cancel the plane wave assembly traction from the flaw surfaces in the expanding wedge-shaped regions exterior to the first set of regions. In these expressions

$$t = t_k = \frac{1}{\vec{v}_k\sqrt{A_\mathrm{i}}}\left(\frac{|y|}{\sqrt{B_k}}\sqrt{A_\mathrm{i} - c_{rk}^2\cos^2\psi} - x + \frac{C_k}{B_k} y\right) \quad (k = 1, 2) \tag{44}$$

locate the planar fronts of these waves; (44) follows from (17b) and (17c) when $(v_\mathrm{r}, \psi_\mathrm{r}, v_\mathrm{t}, \psi_\mathrm{t})$ are eliminated in terms of (v, ψ). The limitations on (x, y) identify the middle term in (41) as a head wave displacement in a wedge-shaped region. Its planar front is defined by

$$t = t_\mathrm{h} = s_1\left(x - \frac{C_2}{B_2} y\right) - \frac{\sqrt{\Gamma_2}}{B_2} y\sqrt{s_2^2 - s_1^2} \tag{45}$$

Similar results follow when $s_1 > s_2$, except that now the head wave arises in w_1^s.

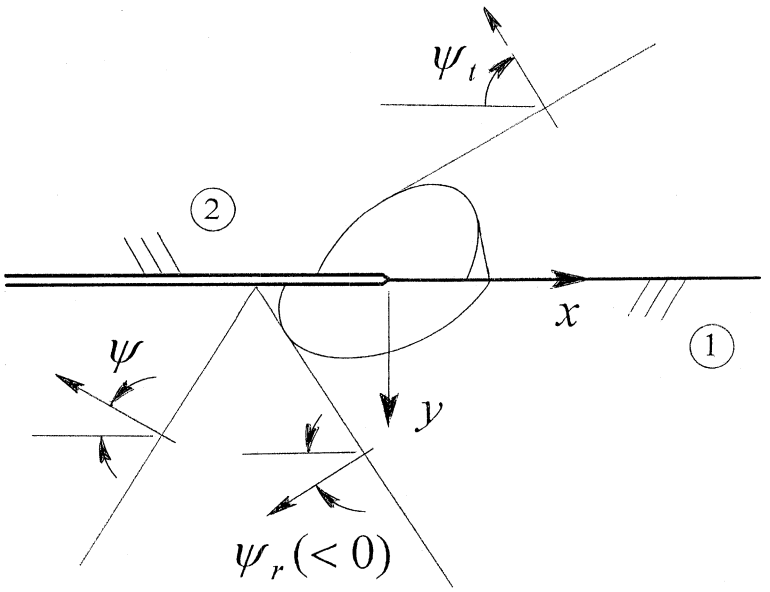

Fig. 2. Schematic of wave diffraction at flaw edge $(t > 0)$.

A schematic of the various wavefronts (incident, reflected, transmitted, scattered) is given in Fig. 2. It is noted that the expanding regions $(y > 0, t > s_1 r_1)$ and $(y < 0, t > s_2 r_2)$ are elliptical in shape. They are centered at the flaw edge, and their semi-major and semi-minor axes correspond to the principal material axes in each solid. The axis tilts with respect to the interface are due to the rotations ϕ_k in the guise of the slope parameters C_k/B_k.

8. Traction behavior near the flaw edge

Superposition gives the interface traction as $\Sigma + \sigma^0_{yz}$ $(y = 0, x > 0)$. Results for Σ near $(x \to 0+)$ the flaw edge can be obtained directly from (35a) or its counterpart for $s_1 > s_2$ by allowing $|q| \to \infty$ and keeping only the highest-order terms. The result is easily inverted with (39) and standard tables (Peirce and Foster, 1956; Sneddon, 1972):

$$\Sigma = \frac{A_0 \Gamma_2^{1/4}}{\pi\sqrt{x}} \frac{G_+(s_\psi)}{a_2^+(s_\psi)} \int_0^t \frac{T(\tau)\,\mathrm{d}\tau}{\sqrt{t-\tau}} + \mathrm{O}(1) \quad (y = 0, x \to 0+) \tag{46}$$

Clearly this term dominates the plane wave assembly contribution σ^0_{yz}, and the coefficient of $1/\sqrt{x}$ is the dynamic stress intensity factor.

9. Solution behavior: two cases

For insight into the effects of non-orthotropy, two simple but non-standard cases are considered.

Case A: The principal axis orientation for incident wave-bearing solid 1 is defined by (38a). Solid 2 is isotropic, but its properties closely match those of solid 1 in the sense that $l = m = 1$. That is, the densities are identical, the average modulus in solid 1 and the classical modulus in solid 2 match, and the interface shear wave speed in solid 1 is either a maximum or a minimum. In view of (21)–(24), (38a) and (38b)

$$\psi_\mathrm{r} = -\psi \quad (\phi_1 = \phi_1^\pm, 0 < \psi < 90^\circ) \tag{47a}$$

$$\psi = \psi^+, \quad \psi^\pm = \tan^{-1}\sqrt{\frac{1 \pm \sqrt{1-\Gamma_1}\cos 2\psi}{\cos^2\psi} - 1} \qquad (\phi_1 = \phi_1^+, 0 < \psi < 90^\circ) \tag{47b}$$

$$\psi_\mathrm{t} = \psi^- \quad \left(\phi_1 = \phi_1^-, \sin^{-1}\sqrt{\frac{\sqrt{1-\Gamma_1}}{1+2\sqrt{1-\Gamma_1}}} < \psi < 90^\circ\right) \tag{47c}$$

Table 2 (Panels A and B) provides data for (47b) and (47c) for various values of $\gamma_1 \geqslant 0$ when $(\alpha_1 = \beta_1, \beta_1 = 2\alpha_1)$, respectively. The entries show that non-orthotropic $\to$ isotropic transmission of the incident wave involves an increasing change in travel direction as the degree of non-orthtropy γ_1 is increased. It should be noted that an exception occurs for $\psi = 45^\circ$; then both possible travel directions are also 45°. Missing entries for ψ^- reflect that the inequality in (47c) is violated; that is, a transmitted wave is precluded for a given combination (ψ, γ_1).

For the less-restrictive $(0 < \psi < 90^\circ)$ case of the maximum interface shear wave speed $(\phi_1 = \phi_1^+, c_{r1} = c_1^+)$ formula (46) reduces to

Table 2
Case A: transmitted wave angles for maximum (+) and minimum (−) interface shear wave speeds vs. (γ_1, ψ)

γ_1	15°: ψ^+ (°)	15°: ψ^- (°)	30°: ψ^+ (°)	30°: ψ^- (°)	60°: ψ^+ (°)	60°: ψ^- (°)	75°: ψ^+ (°)	75°: ψ^- (°)
Panel A: $\alpha_I = \beta_I$								
0.05	19	9.1	31.2	28.7	59.6	60.4	74.7	75.3
0.1	22.1	–	32.3	27.3	59.1	60.8	74.3	75.6
0.25	28.9	–	35.3	22.2	57.7	61.9	73	76.4
0.5	36.2	–	39.2	0.0	54.7	63.4	69.9	77.5
0.75	41.2	–	42.4	–	50.8	64.8	64	78.4
0.9	43.6	–	44	–	47.6	65.5	56.6	78.8
Panel B: $\beta_I = 2\alpha_I$								
0.05	31.8	–	36.8	18.2	56.7	62.4	72.1	76.8
0.1	32.2	–	37	17.7	56.6	62.5	72	76.9
0.25	34.1	–	38	13.3	55.8	62.9	71.1	77.2
0.5	38.4	–	40.6	–	53.3	64	68.1	77.9
0.75	42.4	–	43.2	–	49.4	65	61.2	78.6
0.9	44.4	–	44.6	–	46.1	65.7	51	79

$$\Sigma = \frac{K}{\pi\sqrt{x}} \int_0^t \frac{T(\tau)\,\mathrm{d}\tau}{\sqrt{t-\tau}} + \mathrm{O}(1) \quad (y = 0, x \to 0+) \tag{48}$$

Here the dynamic stress intensity factor coefficient K is given by

$$K = \frac{2\sqrt{\vec{v}_1}F\sin\psi}{M\sqrt{1+\sqrt{M}\cos\psi}} \frac{(1-\sqrt{1-\Gamma_1})\sqrt{M-\cos^2\psi}}{(1-\sqrt{1-\Gamma_1})\sin\psi + \sqrt{M-\cos^2\psi}} \tag{49a}$$

$$M = 1 + \sqrt{1-\Gamma_1}\cos 2\psi \tag{49b}$$

$$\ln F = \frac{1}{\pi}\int_1^{c_1^+} \tan^{-1}\frac{1}{\sqrt{\Gamma_1}}\sqrt{\frac{(c_1^+)^2-\tau^2}{\tau^2-1}}\frac{\mathrm{d}\tau}{\tau + c_1^+\sqrt{M}\cos\psi} \tag{49c}$$

The purely isotropic limit of (48) arises for the diffraction of a plane SH-wave by a crack in a homogeneous material. Eq. (48) then has the factor $K_0 = \sqrt{v_0}\sqrt{1-\cos\psi}$, where v_0 is the classical (Achenbach, 1973) shear wave speed. The matching conditions $l = m = 1$ guarantee that $\vec{v}_1 = v_0$, so that the dimensionless ratio

$$\frac{K}{K_0} = \frac{2F\sqrt{1+\cos\psi}}{M\sqrt{1+\sqrt{M}\cos\psi}} \frac{(1-\sqrt{1-\Gamma_1})\sqrt{M-\cos^2\psi}}{(1-\sqrt{1-\Gamma_1})\sin\psi + \sqrt{M-\cos^2\psi}} \tag{50}$$

varies only with(ψ, Γ_1). It can be demonstrated that

$$0 < \frac{K}{K_0} < 1, \quad \frac{\mathrm{d}}{\mathrm{d}\Gamma_1}\left(\frac{K}{K_0}\right) \geqslant 0 \quad (0 < \Gamma_1 < 0); \qquad \frac{K}{K_0} \to 0 \quad (\Gamma_1 \to 0) \tag{51a, b}$$

Relation (50) and (51a,b) imply that the diffraction of the plane SH-wave in the non-orthotropic/isotropic system produces a smaller dynamic stress intensity factor than diffraction in the homogeneous isotropic material. Moreover, the difference increases as non-orthotropy is increased $(\gamma_1 \to 1, \Gamma_1 \to 0)$. Thus, even when the properties of the bimaterial are similar, i.e. $l = m = 1$, proper orientation of the non-orthotropic constituent can perhaps give an advantage in avoiding fracture over a homogeneous solid identical to the isotropic constituent.

Case B: Now take solid 1 as isotropic, with $l = m = 1$, and the principal axis orientations and interface shear wave speed parameters given by (38a) and (38b). In this instance,

$$\psi_r = -\psi \quad (\phi_2 = \phi_2^{\pm}, 0 < \psi < 90^\circ) \tag{52a}$$

$$\psi_t = \psi^+ \quad \left(\phi_2 = \phi_2^+, \sin^{-1}\sqrt{\frac{1-\Gamma_2}{1+\sqrt{1-\Gamma_2}}} < \psi < 90^\circ\right) \tag{52b}$$

$$\psi_t = \psi^-, \quad \psi^{\pm} = \sin^{-1}\sqrt{\frac{\sin^2\psi \mp \sqrt{1-\Gamma_2}\cos^2\psi}{1 \mp 2\sqrt{1-\Gamma_2}\cos^2\psi}} \qquad (\phi_2 = \phi_2^-, 0 < \psi < 90^\circ) \tag{52c}$$

Table 3 (Panels A and B) provide data for (52b) and (52c) for various values of $\gamma_2 > 0$ when ($\alpha_2 = \beta_2, \beta_2 = 2\alpha_2$), respectively. Entries show that isotropic → non-orthotropic incident wave transmission, like its case A converse, involves an increasing deviation of incident and transmitted wave travel directions as non-orthotropy is increased. An exception occurs again for $\psi = 45^\circ$, when $\psi^{\pm} = 45^\circ$, and missing entries show that wave transmission is precluded when, in this instance, restrictions (52b) arise for the maximum interface shear wave speed case.

For the less-restrictive ($0 < \psi < 90^\circ$) case of minimum shear wave speed, the dimensionless ratio (50) is now

$$\frac{K}{K_0} = \frac{2F(1-\sqrt{1-\Gamma_2})^{1/4}\sqrt{1+\cos\psi}}{\sqrt{1+\sqrt{1-\sqrt{1-\Gamma_2}\cos\psi}}} \frac{M\sqrt{1+\sqrt{1-\Gamma_2}}}{\sin\psi + \sqrt{M}\sqrt{1+\sqrt{1-\Gamma_2}}} \tag{53a}$$

$$M = \sin^2\psi + \sqrt{1-\Gamma_2}\cos^2\psi \tag{53b}$$

$$\ln F = \frac{1}{\pi}\int_1^{1/c_2^-} \tan^{-1}\sqrt{\Gamma_2}\sqrt{\frac{(1/c_2^-)^2 - \tau^2}{\tau^2 - 1}}\frac{d\tau}{\tau + \cos\psi} \tag{53c}$$

Here $\vec{v}_2 = v_0$, and (51a,b) again holds, but with Γ_1 replaced by Γ_2. Thus, increasing the degree of non-orthotropy again decreases the dynamic stress intensity factor below the value achieved for diffraction in a

Table 3
Case B: transmitted wave angles for maximum (+) and minimum (−) interface shear wave speeds vs. (γ_2, ψ)

γ_2	15°: ψ^+ (°)	15°: ψ^- (°)	30°: ψ^+ (°)	30°: ψ^- (°)	60°: ψ^+ (°)	60°: ψ^- (°)	75°: ψ^+ (°)	75°: ψ^- (°)
Panel A: $\alpha_2 = \beta_2$								
0.05	8.6	18.8	28.6	31.1	60.4	59.6	75.3	74.7
0.1	–	21.6	27	32.1	60.9	59.2	75.7	74.4
0.25	–	26.9	18.4	34.3	62.4	58.2	76.8	73.5
0.5	–	31.7	–	36.7	65.9	56.8	79.1	72.1
0.75	–	34.4	–	38.2	71.6	55.7	82.2	71
0.9	–	35.6	–	38.9	77.7	55.1	85	70.3
Panel B: $\beta_2 = 2\alpha_2$								
0.05	–	28.9	–	35.3	63.5	57.7	77.5	73
0.1	–	29.2	–	35.4	63.6	57.6	77.6	72.9
0.25	–	30.4	–	36	64.6	57.2	78.3	72.6
0.5	–	33	–	37.4	67.8	56.3	80.2	71.6
0.75	–	35	–	38.5	74	55.4	83.3	70.6
0.9	–	36	–	39.1	82	54.9	86.8	70.1

homogeneous isotropic solid. Again, the bimaterial factor vanishes when the non-orthotropy parameter reaches its limit value of unity.

10. Some comments

This article considered the diffraction of a plane SH-wave by an interface flaw in a bimaterial consisting of two non-orthotropic linearly elastic solids. Each solid had only a single plane of material symmetry and, while these coincided, orientations of the principal material axes in the common plane were arbitrary, both with respect to each other and with respect to the interface and the direction of travel of the SH-wave.

An exact transient analysis gave the full-field displacements in each solid, and the interface traction just ahead of the flaw edge. These expressions and related formulas showed that the speeds of the incident, reflected and transmitted plane waves, and the travel directions of the latter two with respect to the former, are sensitive to the principal material axis orientations, as well as the elastic properties themselves. Study of the scattered wave field showed that this sensitivity is also manifest in the shear wave speeds in each solid. Principal material axis orientations for each solid were readily found that guaranteed maximum and minimum speeds along the interface. Calculations showed that the maximum and minimum values lay, respectively, above and below the isotropic limit, and that deviations from the limit increased with the degree of non-orthotropy.

To focus on the effects of non-orthotropy and material orientation, results were specialized for two cases of a non-orthotropic/isotropic bimaterial. In one, the incident wave arose in the homogeneous solid; in the other, plane wave transmission was into the homogeneous solid. In both cases, the non-orthotropic and isotropic properties closely matched, and the principal axis orientations for the non-orthotropic solid were chosen to give maximum or minimum shear wave speeds along the interface. Calculations for both cases showed that deviation in the travel directions of the incident and transmitted plane waves increased with the degree of non-orthotropy, and that non-orthotropy by itself might preclude plane wave transmission.

The dynamic stress intensity factors for these two illustrations showed analogous behavior: Their values always lay below that for plane wave diffraction in a homogeneous solid of a material identical to that of the isotropic constituent of the bimaterial. The discrepancy increased with non-orthotropy, and the bimaterial factor could indeed be forced to zero when non-orthotropy reached a theoretical limit.

Control of elastic wave transmission and prevention of diffraction-induced dynamic failure in layered solids are common research topics (Liu et al., 2001; Ma et al., 2001), and use of elastic property mismatching is a well-known aspect of these (Brock and Achenbach, 1973). It is hoped that the present study has demonstrated, both through its exact results and somewhat general model, and its examination of two special cases, the importance of considering material orientation and non-orthotropy.

The class of materials considered here lends itself well to anti-plane strain situations. While useful for insight, these are generally not as applicable as in-plane loading situations. For that reason alone, the exact results presented here were not fully exploited through e.g. use of more general parameter variations. As noted by Eshelby et al. (1953), certain tractable in-plane situations can also be studied for this material class. Interface flaw work is underway on some of these, as well as for standard (Payton, 1983; Brock et al., 2001; Brock and Hanson, in press) transversely isotropic and orthotropic materials. The present analysis is serving as a guide.

References

Achenbach, J.D., 1973. Wave Propagation in Elastic Solids. North-Holland, Amsterdam.

Brock, L.M., Achenbach, J.D., 1973. Extension of an interface flaw under the influence of transient waves. International Journal of Solids and Structures 9, 53–68.

Brock, L.M., Hanson, M.T., in press. An exact transient analysis of plane wave diffraction in an orthotropic or transversely isotropic solid. International Journal of Solids and Structures.

Brock, L.M., Georgiadis, H.G., Hanson, M.T., 2001. Rapid indentation of transversely isotropic or orthotropic half-spaces. ASME Journal of Applied Mechanics 68, 490–495.

de Hoop, A.T., 1960. A modification of Cagniard's method for solving seismic pulse problems. Applied Scientific Research B 8, 349–356.

Eshelby, J.D., Read, W.T., Shockley, W., 1953. Anisotropic elasticity with applications to dislocation theory. Acta Metallurgica 1, 251–259.

Kraut, E.A., 1963. Advances in the theory of anisotropic wave propagation. Reviews of Geophysics 1, 401–488.

Liu, G.R., Han, X., Lam, K.Y., 2001. Material characterization of FGM plates using elastic waves and an inverse procedure. Journal of Composite Materials 35, 954–971.

Ma, C.-C., Liu, S.-W., Lee, G.S., 2001. Dynamic responses of layered medium subjected to anti-plane loadings. International Journal of Solids and Structures 38, 9295–9312.

Miklowitz, J., 1978. The Theory of Elastic Waves and Waveguides. North-Holland, Amsterdam.

Noble, B., 1958. Methods Based on the Wiener–Hopf Technique. Pergamon, New York.

Nye, J.F., 1957. Physical Properties of Crystals, Their Representation by Tensors and Matrices. Clarendon Press, Oxford.

Payton, R.G., 1983. Elastic Wave Propagation in Transversely Isotropic Solids. Martinus Nijhoff, The Hague.

Peirce, B.O., Foster, R.M., 1956. A Short Table of Integrals. Blaisdell, Waltham, MA.

Sneddon, I.N., 1972. The Use of Integral Transforms. McGraw-Hill, New York.

Sokolnikoff, I.S., 1956. Mathematical Theory of Elasticity. McGraw-Hill, New York.

Theocaris, P.S., Sokolis, D.P., 2000. Invariant elastic constants and eigentensors of orthtorhombic, hexagonal and cubic crystalline materials. Acta Crystallographica A 56, 310–331.

van der Pol, B., Bremmer, H., 1950. Operational Calculus Based on the Two-Sided Laplace Integral. Cambridge University Press, UK.